Title
Molecular Insights into the Mechanisms of SUN1 Oligomerization in the Nuclear Envelope

Journal
Biophysical Journal, 114(5)

ISSN
0006-3495

Authors
Jahed, Zeinab
Fadavi, Darya
Vu, Uyen T
et al.

Publication Date
2018-03-01

DOI
10.1016/j.bpj.2018.01.015

Peer reviewed

Biophysical Journal
Article

Biophysical Society

Molecular Insights into the Mechanisms of SUN1 Oligomerization in the Nuclear Envelope

Zeinab Jahed,[1] Darya Fadavi,[1] Uyen T. Vu,[1] Ehsaneddin Asgari,[1] G. W. Gant Luxton,[2] and Mohammad R. K. Mofrad[1,3,*]

[1]Molecular Cell Biomechanics Laboratory, Departments of Bioengineering and Mechanical Engineering, University of California, Berkeley, Berkeley, California; [2]Department of Genetics, Cell Biology, and Development, University of Minnesota, Minneapolis, Minnesota; and [3]Molecular Biophysics and Integrated Bioimaging Division, Lawrence Berkeley National Laboratory, Berkeley, California

ABSTRACT The LINC complex is found in a wide variety of organisms and is formed by the transluminal interaction between outer- and inner-nuclear-membrane KASH and SUN proteins, respectively. Most extensively studied are SUN1 and SUN2 proteins, which are widely expressed in mammals. Although SUN1 and SUN2 play functionally redundant roles in several cellular processes, more recent studies have revealed diverse and distinct functions for SUN1. While several recent in vitro structural studies have revealed the molecular details of various fragments of SUN2, no such structural information is available for SUN1. Herein, we conduct a systematic analysis of the molecular relationships between SUN1 and SUN2, highlighting key similarities and differences that could lead to clues into their distinct functions. We use a wide range of computational tools, including multiple sequence alignments, homology modeling, molecular docking, and molecular dynamic simulations, to predict structural differences between SUN1 and SUN2, with the goal of understanding the molecular mechanisms underlying SUN1 oligomerization in the nuclear envelope. Our simulations suggest that the structural model of SUN1 is stable in a trimeric state and that SUN1 trimers can associate through their SUN domains to form lateral complexes. We also ask whether SUN1 could adopt an inactive monomeric conformation as seen in SUN2. Our results imply that the KASH binding domain of SUN1 is also inhibited in monomeric SUN1 but through weaker interactions than in monomeric SUN2.

INTRODUCTION

Linkers of nucleoskeleton and cytoskeleton (LINC) are conserved molecular bridges spanning the nuclear envelope (NE) that provide a direct physical linkage between major cytoskeletal and nucleoskeletal elements (1–4). The ability of LINC complexes to sense and transmit cytoskeletal forces across the NE is critical for several fundamental cellular processes, including meiotic chromosome pairing, mechanotransduction, and nuclear positioning (5–7). Given the prominent roles of LINC complexes in basic cellular functions, it should not be surprising that mutations in genes encoding their components are associated with a wide range of diseases and disorders, including cardiac and skeletal muscular disorders (8–16), cancers (10,17), and hearing loss (18).

LINC complexes are composed of the conserved inner nuclear membrane (INM) and outer nuclear membrane *Sad1/UNC-84* (SUN) and *Klarsicht/ANC-1/SYNE* homology (KASH) proteins, respectively (3). Also known as NE spectrin repeat proteins (nesprins), KASH proteins are type II membrane proteins that project their divergent spectrin-repeat-containing N-termini from the outer nuclear membrane into the cytoplasm, where they interact with the cytoskeleton and other cytoplasmic proteins (19). Within the perinuclear space of the NE, KASH proteins protrude their eponymous ~10–32 residue KASH peptide (1). SUN proteins are membrane proteins that are defined by their luminal KASH peptide-binding C-terminal SUN domain (20,21). The divergent N-termini of SUN proteins reside within the nucleoplasm, where they interact with A-type lamins, chromatin, and other INM proteins (22). Mammals encode at least six KASH protein-encoding genes (nesprin-1–4, lymphoid-restricted membrane protein, and KASH5) and five SUN protein-encoding genes (SUN1-5), which are expressed in a tissue-specific manner and are subject to alternative splicing (23–26).

SUN1 and SUN2 are the most widely expressed mammalian SUN proteins and can interact with the KASH peptides of at least four KASH proteins (nesprin-1–4) (4,5,27–30). SUN1 can additionally interact with KASH5 during mammalian meiosis (31). The promiscuity of SUN1 and

Submitted August 11, 2017, and accepted for publication January 17, 2018.

*Correspondence: mofrad@berkeley.edu

Editor: Jason Swedlow.

https://doi.org/10.1016/j.bpj.2018.01.015

SUN2 for KASH proteins is consistent with previous reports of their partial functional redundancy during centrosome-nucleus coupling in neuronal precursors in the developing brain, DNA damage repair, nuclear anchorage in skeletal muscle, and interkinetic nuclear migration in photoreceptor progenitor cells of the developing retina (28,30,32,33). However, evidence of specific functions for SUN1- and SUN2-containing LINC complexes also exists in the literature (23,34–36). For example, SUN1 is required for DNA double-strand break repair, meiotic chromosome pairing, messenger RNA export, nuclear pore complex insertion into and distribution throughout the NE, and nucleolar morphogenesis (17,35–39). In addition, linear arrays of SUN2-containing LINC complexes assemble on perinuclear actin cables to form transmembrane actin-associated nuclear lines that move the nucleus rearward in migrating fibroblasts and myoblasts (22,40). Currently, the molecular mechanisms responsible for these dissimilar SUN1- and SUN2-containing LINC complex functions remain poorly understood.

Early on in the discovery of LINC complexes, structure prediction algorithms detected coiled coil (CC) regions in the luminal domains of SUN1 and SUN2, implying that these proteins oligomerize to perform their functions in the NE (2,3). Subsequently, various experimental techniques were employed to determine the oligomeric state of these proteins and to identify the regions involved in their oligomerization, often yielding contradicting results (summarized in Table 1). For example, early studies using in vitro binding assays and coimmunoprecipitation found that full-length human SUN2 forms homodimers (41). Similarly, mouse and human SUN1 were shown to form

TABLE 1 Summary of Studies on SUN1 and SUN2 Protein Oligomerization

Region	Residue Range	SUN Protein	KASH Binding	Oligomer State	Species	Method and/or Environment	Year and Reference
Predicted CC2 and SUN domain	336–717	SUN2	–	dimer[a]	human	in vitro binding assay and coimmunoprecipitation	2006 (41)
Predicted CC1-CC2 and SUN domain	433–717	SUN2	–	dimer[a]	human	in vitro binding assay and coimmunoprecipitation	2006 41)
Full length		SUN2	–	dimer[a]	human	in vitro binding assay and coimmunoprecipitation	2006 (41)
Full luminal domain without SUN domain	432–737	SUN1	–	dimer and tetramer	mouse	native PAGE	2008 (34)
Full length		SUN1	–	monomer, dimer, and tetramer	human	Western blot	2008 (34)
α3-SUN	519–716	SUN2	yes	monomer and trimer mix	human	size-exclusion chromatography, SDS-PAGE gel, and Western blotting	2012 (43,44)
α3-SUN	519–716	SUN2	yes	trimer	human	crystallization (PDB : 3unp)	2012 (43,44)
UCC and α3-SUN	UCC-522–717[b]	SUN2	yes	trimer	human	SDS-PAGE crystallization (PDB : 4dxt, 4dxs)	2012 (42)
α3-SUN	522–717	SUN2	no	–	human	SDS-PAGE	2012 (42)
Almost the entire luminal domain	335–717	SUN2	no	trimer	human	analytical ultracentrifugation (sedimentation equilibrium)	2012 (42)
CC1	378–450[c]	SUN2	no	trimer	mouse	analytical gel-filtration analysis, chemical cross-linking assay, and size-exclusion chromatography crystallization (PDB : 5ed9)	2016 (46)
CC2-SUN domain	451–699[c]	SUN2	no	monomer	mouse	analytical gel-filtration analysis, chemical cross-linking assay, and size-exclusion chromatography crystallization (PDB : 5ed8)	2016 (46)
CC2 (includes α1, α2, and α3)	451–523[c]	SUN2	no	monomer	mouse	analytical gel-filtration analysis, chemical cross-linking assay, and size-exclusion chromatography	2016 (46)
CC1-CC2	378–523[c]	SUN2	no	trimer	mouse		
SUN	524–699	SUN2	no	monomer	mouse		
CC1-CC2-SUN	378–523[c]	SUN2	yes	monomer and trimer mix	mouse		
α3-SUN	~501–699[c]	SUN2	–	monomer and trimer mix	mouse	analytical gel-filtration analysis	2016 (46)

CC1, Coiled coil 1; CC2, Coiled coil 2; PAGE, polyacrylamide gel electrophoresis; SDS-PAGE, sodium dodecyl sulfate polyacrylamide gel electrophoresis; UCC, unrelated trimeric coiled coil.

[a]In their discussion, Wang et al. (41) also suggest that the SUN2 protein may form a complex of a dimer or a trimer under certain experimental conditions, but this data was not shown in their article.

[b]Although residues 522–717 are trimers in the crystalized structure, a nonrelated CC of GCN4 was fused to this fragment for crystallography. The SUN2 522–717 fragment alone is unable to bind KASH and was therefore predicted to be a monomer by Sosa et al. (42) without the fusion of this unrelated CC.

[c]These residue numbers correspond to mouse SUN2 isoform 3, which has a length of 699 and is missing residues 154–185 from the canonical sequence (46).

dimers or tetramers using gel electrophoresis and Western blotting, respectively (34). Ultimately however, crystal structures of a short fragment of human SUN2 in a complex with KASH2 peptides revealed a trimeric SUN domain preceded by an α-helix (α3) (Fig. 1 *A*) that could simultaneously bind to three KASH peptides (42–44). In this structure, each KASH peptide was bound in a groove formed by a highly conserved KASH lid extending from the SUN domain and the SUN domain of its neighboring protomer (Fig. 1, *A* and *B*). Some of these studies suggested that the α3-SUN domain fragment is sufficient for trimerization and KASH binding in SUN2 (43,44), whereas others showed that SUN domain trimerization is only enabled by CCs preceding this solved region (Fig. 1 *A*) (42,45,46) (Table 1). More recently, Nie et al. (46) solved the structure of a larger fragment of mouse SUN2 containing two additional α-helices (α1 and α2) (Fig. 1 *C*). In this conformation, the KASH lid is bound between a three-helix bundle formed by α1, α2, and α3, keeping the SUN domain monomeric and inactive for KASH binding (Fig. 1 *B*). Based on the abovementioned structural analyses, the current model of SUN2 oligomerization in the NE proposes an inactive SUN2 in a monomeric form, which is activated by the trimerization of at least the SUN domain and α3 helices

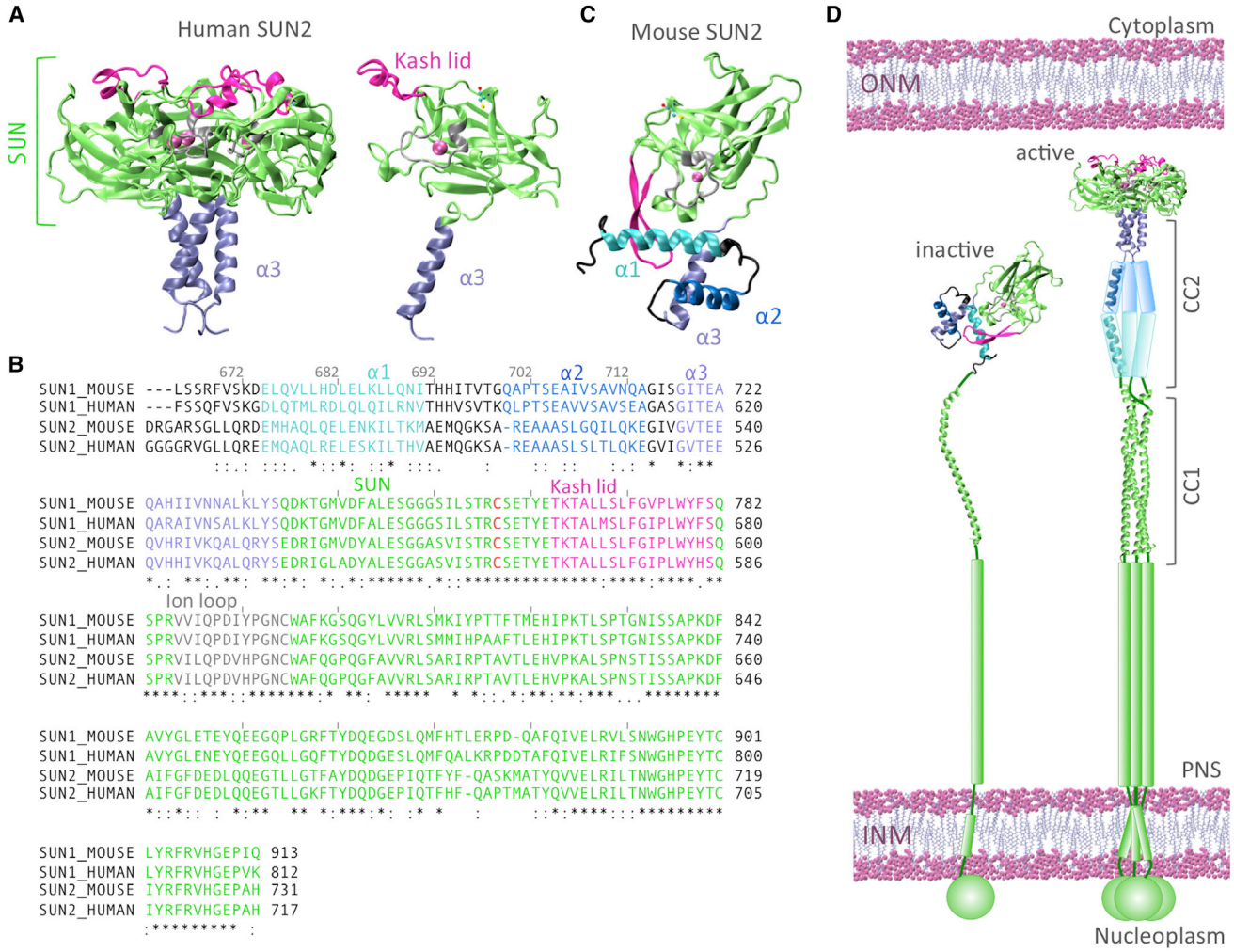

FIGURE 1 Structures and sequences of SUN domain proteins SUN1 and SUN2. (*A*) Shown are the crystal structure of homotrimeric human SUN2 (42) (PDB: 4dxt) (*left*) and a representative image of one symmetric unit of this trimer (*right*). (*B*) The sequence alignment of human and mouse SUN1 and SUN2 is shown (47). Important regions identified on the SUN2 crystal structure are colored on the four sequences accordingly. An asterisk (*) indicates positions with fully conserved residues. A colon (:) indicates conservation between groups with strongly similar chemical properties. A period (.) indicates conservation between groups with weakly similar chemical properties (based on Clustal Omega program formatting). Sequence regions are colored based on the aforementioned labels. (*C*) Shown is the crystal structure of monomeric mouse SUN2 (46) (PDB: 5ed8) depicting the autoinhibition of the KASH lid via interaction with the α-1–3 helix bundle. Two α-helices, α1 (*cyan*) and α-2 (*blue*), precede the SUN domain and α3. In this conformation the KASH lid (*magenta*) is hindered by a helix bundle formed by α1, α2 and α3 helices, and KASH binding is reportedly inhibited (46). (*D*) Shown is a working model of SUN2 activation for KASH-binding in the PNS: trimerization of the SUN domain is regulated via CC regions of SUN2 (46) and is an essential step for KASH binding and LINC complex formation. CC1, Coiled coil 1; CC2, Coiled coil 2; ONM, outer nuclear membrane; PNS, perinuclear space. To see this figure in color, go online.

(Fig. 1 *D*) (46). In this model, trimerization is indispensable for KASH binding; however, it remains unclear whether the entire molecule can form trimeric CCs as shown in Fig. 1 *D* (45,46). It should be noted that the crystal structures of monomeric (α1-SUN) and trimeric (α3-SUN) SUN2 are from different species.

Despite these important mechanistic insights into SUN2 oligomerization and KASH peptide binding, the lack of similar structural information for SUN1 has limited progress toward understanding the assembly and regulation of SUN1-containing LINC complexes. However, there is evidence in the literature to suggest that SUN1 may assemble a wider range of homo-oligomers than SUN2. For example, native gel electrophoresis and cross-linking studies have demonstrated the existence of SUN1 homodimers and homotetramers, which form through a combination of CC interactions and interchain disulfide bonds (34). Moreover, recent fluorescence fluctuation spectroscopy and brightness analyses conducted in Dr. Joachim Mueller's laboratory at the University of Minnesota (J.M., personal communication) show that although the luminal domain of SUN2 does homotrimerize in the NE of living cells, the in vivo homo-oligomerization of the SUN1 luminal domain is not limited to a trimer. Here, we applied a multifunctional computational modeling approach to begin to define the assembly mechanism of SUN1 homo-oligomerization to shed light on the functional specification of SUN1- and SUN2-containing LINC complexes.

METHODS

Multiple sequence alignments

Sequence alignments were performed using the Basic Local Alignment Search Tool (47). In all shown alignments, Clustal Omega program formatting was used, where an asterisk (*) indicates positions with fully conserved residues, a colon (:) indicates conservation between groups of strongly similar properties, and a period (.) indicates conservation between groups of weakly similar properties. Sequence similarities were calculated using the Basic Local Alignment Search Tool and reported as percent identities (i.e., the percentage of residues that are identical between the two sequences) and similarities (the percentage of residues with positive substitutions). All residue numberings are based on isoform 1 of the respective SUN protein.

Structural modeling

We generated homology models for mouse SUN1 and SUN2 and human SUN1 trimers using the structure of human SUN2 (Protein Data Bank [PDB]: 4dxt) as a template. We also modeled the inactive conformation of mouse SUN1 based on the inactive structure of mouse SUN2 (PDB: 5ed8). Homology modeling was performed using the SWISS-MODEL servers (48). SWISS-MODEL performs an analysis of pairwise interfaces of the template structure to predict the homo-oligomeric structure of the modeled protein. Based on this, all structures made using the 4dxt and 5ed8 templates were predicted to be trimers and monomers, respectively. Modeled structures were visualized using VMD software (49). They were next solvated in water, neutralized with counterions, and ionized with KCl and $CaCl_2$.

Docking

ZDOCK was used for molecular docking of SUN1 or SUN2 trimers (50). ZDOCK uses an energy-based scoring function to rank the top docking solutions among all binding modes in the translational and rotational space between the molecules. We downloaded the top five solutions for SUN1 and SUN2 for further analysis.

MD simulations

All atom molecular dynamics (MD) simulations were performed using NAMD scalable MD with the CHARMM27 force field (51) on a total of eight systems (summarized in Table S1). All systems were minimized at 5000 steps and equilibrated for ~2 ns with a time step of 2 fs. Simulations were performed under a constant temperature of 310 K and a constant pressure of 1 atm using the Langevin piston method and Hoover's method during minimization and equilibration (51). Additionally, periodic boundary conditions were applied in all three directions. Finally, a total of three independent simulation runs were conducted and analyzed for each system (summarized in Table S1).

RMSD calculations

Per residue and average root mean-square deviation (RMSD) values were computed using the RMSD Visualizer Tool plug-in for the VMD extension and plotted using the R gplot package (R Foundation for Statistical Computing, Vienna, Austria). All frames of the trajectory were aligned to a reference frame (frame 0) before RMSD computations to eliminate the effect of rotation and translation of the molecule during the simulation. For lateral interaction simulations, we first aligned all frames of the trimer-trimer complex trajectory by using the first frame of one of the trimers as a reference. We then computed the average RMSD of the second trimer with respect to the first trimer.

Energy calculations

Average nonbonded interaction energies and the average number of hydrogen bonds between the regions of interest were evaluated in VMD (http://www.ks.uiuc.edu/Research/vmd/vmd-1.9.1/, version 1.9.1) using NAMD energy (version 1.4) and HBonds (version 1.2) plug-ins, respectively. The cutoff distance was set to 1.2 nm for all nonbonded interactions and 3.5 Å for hydrogen bonds. An angle cutoff of 20 degrees was used for hydrogen bonds. The structural regions selected for energy calculations were based on various conserved domains identified experimentally for SUN2, as shown in Fig. 1 *B*; similar regions were selected on SUN1 based on sequence alignments shown in Fig. 1 *B*.

For pairwise interaction energy calculations in SUN1 lateral trimer-trimer interactions, we first measured pairwise distances between all residues in trimer 1 and trimer 2. We then identified all residues on trimer 1 that consistently maintained a 4 Å distance from trimer 2 over all three simulations trajectories (residues 702, 704, 739, 741, 743, 751, 752, 753, 754, 755, 758, 788, 790, and 791 on human SUN1; Fig. S3). Finally, we computed pairwise nonbonded interaction energies between these residues on trimer 1 and trimer 2 and used the R gplot package to create heat maps via the heatmap.2() function. The total energy (van der Waals (VDW) and electrostatic (ELEC)) fluctuations over MD simulation time are provided in the supplementary figures where relevant (Figs. S1 and S4).

Angle calculations

Angles were calculated between various segments of SUN1 or SUN2 (α1, α2, α3, and the KASH lid) by representing each segment as a vector. On each α-helix, a vector was drawn through two conserved residues near

the ends of the helices. Similarly, the KASH lid was represented with a vector passing through two conserved residues on one of its beta strands. The angles were then calculated between the two corresponding vectors representing α1, α2, α3, and the KASH lid segments of SUN1 or SUN2. All residue pairs used in angle calculations are summarized in Table S2).

RESULTS

Homotrimers are favorable oligomeric states for the SUN and α3 domains of SUN1

Structures of the SUN domains and α3 helices of human SUN1 (SUN1H) and mouse SUN1 (SUN1M) as well as mouse SUN2 (SUN2M) were homology modeled using the crystal structure of human SUN2 (SUN2H; PDB : 4dxt) as a template (48). Because of high sequence similarities between the α-3-SUN fragments of SUN1 and SUN2 (67% identity and 81% similarity) and particularly high conservation of hydrophobic residues at protomer interfaces, the oligomeric state of all modeled structures was predicted to be homotrimeric, similar to the SUN2H template (see Methods) (48). To further test whether the predicted homotrimeric state is favorable in SUN1, and to refine our homology models and compare their dynamics, three independent MD simulations were performed on each of the four resulting structural models, namely SUN1M, SUN2M, SUN1H, and SUN2H. We evaluated the stabilities of our structural models by calculating the deviations of the modeled structures from their initial states at the first timestep of our MD simulations. This was done through calculating average, and per-residue RMSD values of the backbone atoms of each modeled structure, over their MD trajectories (Fig. 2 *A*) (see Methods for details). Additionally, we mapped regions with high RMSD values onto each respective modeled structure (Fig. 2 *A*). The regions of our models corresponding to loops lacking a secondary structure or terminal residues had the highest per-residue RMSD values (RMSD $>$ 3Å), as expected (Fig. 2 *A*). Despite high per-residue RMSD values in these regions, the average RMSD values for all four models reached equilibrium at values below 3 Å over the course of three independent 45 ns simulations (Fig. 2 *A*).

We next performed a one-to-one map of all nonconserved and semiconserved substitutions between SUN1H and SUN2H sequences on their respective refined structural models (Fig. 2, *B* and *C*). The hydrophobic residues (V528, V532, L536, Y539) responsible for trimeric CC formation in SUN2H (52) were conserved in the α3 helices of SUN1H (A622, V626, L630, Y633). Interestingly however, charged residues on the solvent-exposed surface of SUN2H α3 helices (R538, Q534, H530, E526) were substituted with hydrophobic or polar residues on the outer layer of SUN1 α3 helices (L632, S628, A624, A620) (Fig. 2 *B*). A similar analysis of the SUN domains of SUN1H and SUN2H revealed a highly conserved hydrophobic core at the interface between two SUN protomers (Fig. 2 *C*). Most of the nonconserved substitutions were found in solvent-exposed loops in the SUN1H and SUN2H SUN domains (Fig. 2 *C*) and corresponded to the regions with high RMSD values shown in Fig. 2 *A*.

To compare the potential interaction energies at protomer interfaces between SUN1 and SUN2 trimers, we calculated the total nonbonded interaction energies (VDW and ELEC) between regions of neighboring SUN protomers that contribute to trimer formation and compared them across MD trajectories of each model (Fig. 3, *A* and *B*). The total nonbonded protomer-protomer interaction energy is composed of interactions between adjacent SUN domains or α3 helices of neighboring protomers or between the SUN domain of one protomer and the α3 helix of the neighboring protomer (Figs. 3, *A* and *B* and S1). These energies were consistent between all of our four models (Figs. 3, *A* and *B* and S1). We further investigated the interaction between the SUN domain and the α3 helix and identified a salt bridge that is formed between the SUN domain and the α3 helix of neighboring protomers that, to the best of our knowledge, was not highlighted in the structure solved by Sosa et al. (42,45) (Figs. 3 *C* and S1). This interprotomer salt bridge is distinct from the highly conserved intraprotomer salt bridge previously identified between the α3 helix of each protomer and its own SUN domain (D542-R708 pair in SUN2H) (42). In SUN2H, three of these interprotomer salt bridges form between K533 residues on each α3 helix and E672 residues on the SUN domains of adjacent protomers (see Figs. 3, *D* and *E* and S1). Similar interprotomer salt bridges form between residues K547 and E686 at the same positions on our SUN2M model (Figs. 3, *D* and *E* and S1). Despite the absence of lysine residues at this position on SUN1M and SUN1H α3 helices, our models predicted that a lysine found in the α3 helix four residues closer to the SUN domain is positioned perfectly to form a salt bridge with the corresponding residue position on the SUN domains of adjacent protomers (K631-E766 in SUN1H and K733-D868 in SUN1M) (Figs. 3, *D* and *E* and S1).

To determine the contribution of the identified interprotomer salt bridges to the overall potential energy of the modeled SUN1 and SUN2 protomer interfaces, we calculated the nonbonded interaction energies between the salt-bridge-forming residue pairs (Figs. 3 *D* and S1). These energies were equal in value to the interaction energies between the SUN domains and neighboring α3 helices shown in Fig. 3 *B*, indicating that the identified interprotomer salt bridges are the sole interprotomer interactions between SUN domains and neighboring α3 helices. In addition to nonbonded energies, we quantified the number of hydrogen bonds that formed between these residue pairs during a 45 ns MD simulation (Figs. 3 *C* and S1). Taken together, these results strongly suggest that like SUN2, the α3-SUN domain fragment of SUN1 favors a trimeric state.

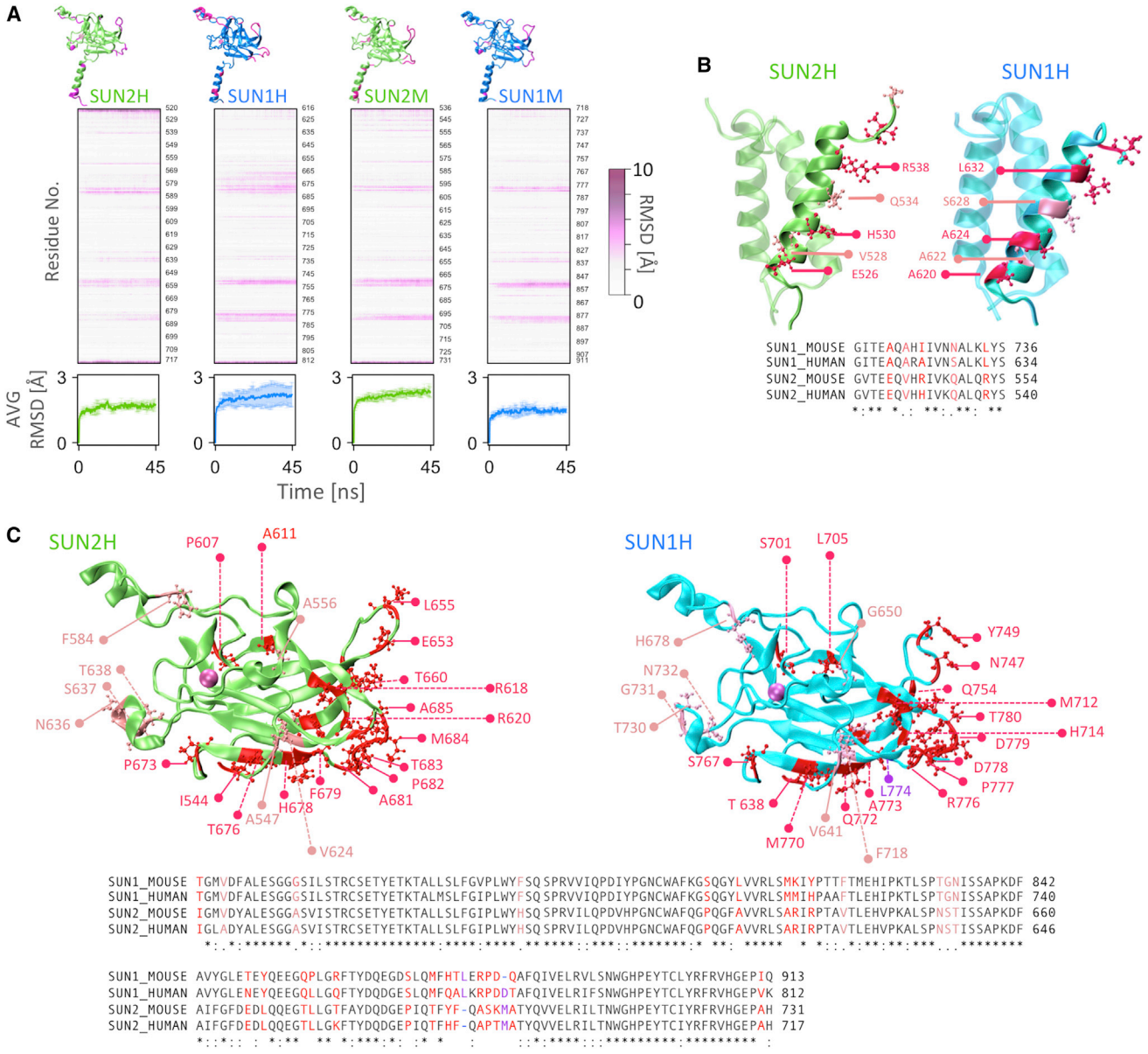

FIGURE 2 Structural model of SUN1 based on the structure of SUN2. (*A*) The RMSD of SUN1H, mouse SUN1 (SUN1M), human SUN2 (SUN2H), and mouse SUN2 (SUN2M) structural models is shown. Heatmaps show the per-residue Cα-atom RMSD over time for SUN2 (*green*) and SUN1 (*blue*) relative to the initial minimized modeled structures (*top*). High RMSD regions are mapped onto the crystal structure of each model and shown above each heatmap. The average Cα-atom RMSD for SUN2 (*green*) and SUN1 (*blue*) relative to the initial minimized modeled structures (*bottom*) is shown. All frames of the simulation were first aligned to the initial frame before calculating the RMSD. Averages were obtained from three independent simulation runs. (*B*) Shown is a one-to-one map of nonconserved residue substitutions in the α-3 helix between SUN1H and SUN2H. Nonconserved residue substitutions on SUN1 compared with SUN2 are colored in red, semiconserved residues in pink, and additional residues in purple. (*C*) Shown is a one-to-one map of nonconserved residue substitutions between the SUN domains of SUN1H and SUN2H. AVG, average. To see this figure in color, go online.

SUN1 forms stable lateral trimer-trimer interactions, whereas SUN2 does not

Our models predict that the α3-SUN domain of SUN1 can homotrimerize similarly to SUN2, so we next sought to investigate how SUN1 homotrimers might be assembled into higher-order oligomers as observed experimentally (J.M., personal communication) (34). Previously, SUN proteins were hypothesized to form an extended network in the NE through lateral interactions between the CCs and SUN domains of adjacent homotrimers (43,44). To test this hypothesis, we performed molecular docking on the equilibrated structural models of SUN1 and SUN2 homotrimers (50).

The results of our initial docking experiments revealed a propensity for SUN protein homotrimers to interact

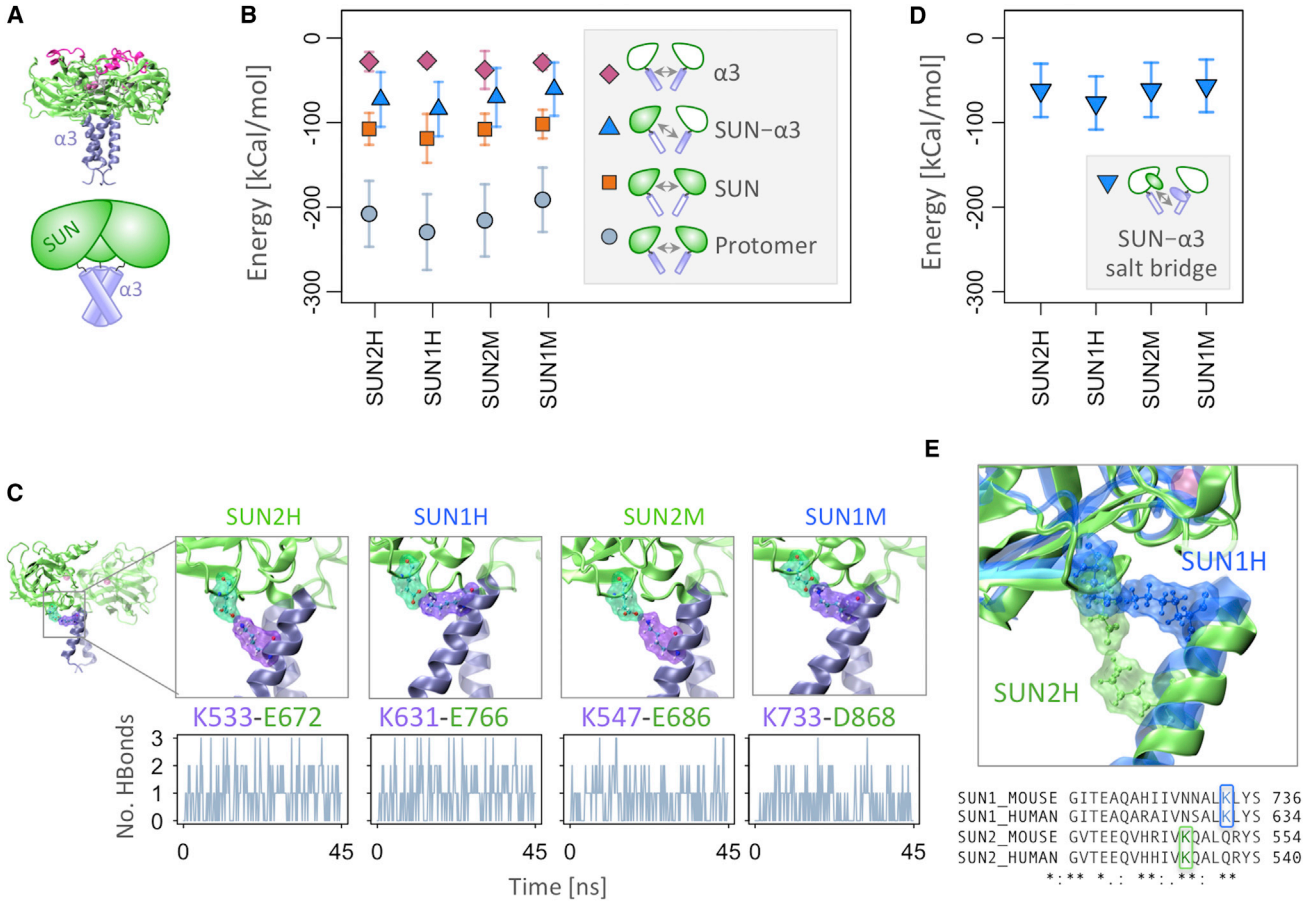

FIGURE 3 Molecular dynamics of SUN1 and SUN2 homotrimers. (*A*) Shown is an illustration of the human SUN2 trimer domain architecture: the SUN domains are shown in green, and CC-forming α3 helices are shown in purple. (*B*) Shown are calculated nonbonded interaction energies between the indicated structural regions. (*C*) Shown are interprotomer salt bridges between the SUN domain of each protomer and the a3 helix of an adjacent protomer (top) and the number of hydrogen bonds between the interprotomer salt-bridge-forming residue pairs (bottom). (*D*) Shown are calculated nonbonded interaction energies between interprotomer salt-bridge-forming residue pairs. Nonbonded interaction energies are averaged over MD simulation time and three independent runs, and error bars correspond to one standard deviation. (*E*) Shown is a superimposed structure of one α3 helix and a neighboring SUN domain on SUN1H and SUN2H homotrimers with the salt-bridge-forming residue side chains depicted. HBond, hydrogen bond. To see this figure in color, go online.

head-to-head via interactions between their KASH lids (Fig. S2). This is unlikely to occur in vivo, as both SUN trimers are anchored to the inner NE. Therefore, we manually blocked the KASH lids from interacting and repeated docking. Four of the top five SUN1 docking solutions (1, 2, 4, and 5) revealed lateral associations between the SUN domains of adjacent homotrimers (Fig. 4 *A*) (see Methods). However, no such docking solutions were observed for SUN2. Although three of the five SUN2 docking solutions (1, 3, and 5) involved SUN domain interactions, they did not result in parallel lateral interactions between neighboring homotrimers. A similar arrangement was observed in the remaining docking solution of SUN1 (3). In addition, the remaining two docking solutions for SUN2 (2 and 4) were mediated by interactions between the SUN domain and CCs, which resulted in an antiparallel homotrimer arrangement unlikely to occur in vivo.

Next, to observe the dynamics of such an interaction, we conducted MD simulations on the lateral complex solution obtained from molecular docking of SUN1 trimers. For comparison, two SUN2 trimers were also manually positioned into a laterally interacting complex similar to that of the SUN1 trimers. The trace of the position of one SUN homotrimer versus the other one over all MD simulations indicated more variability in the position of SUN2 homotrimers compared with that of SUN1 homotrimers (Fig. 4 B). Correspondingly, the RMSD of one SUN homotrimer versus the other one is higher for SUN2 homotrimers compared with that of SUN1 homotrimers (Fig. 4 *C*) (see Methods for more details). To begin to determine the mechanism responsible for the lateral SUN domain interactions between adjacent SUN1 homotrimers, we identified solvent exposed residues at the homotrimer-homotrimer interface that maintained a 4 Å distance over the course of all three

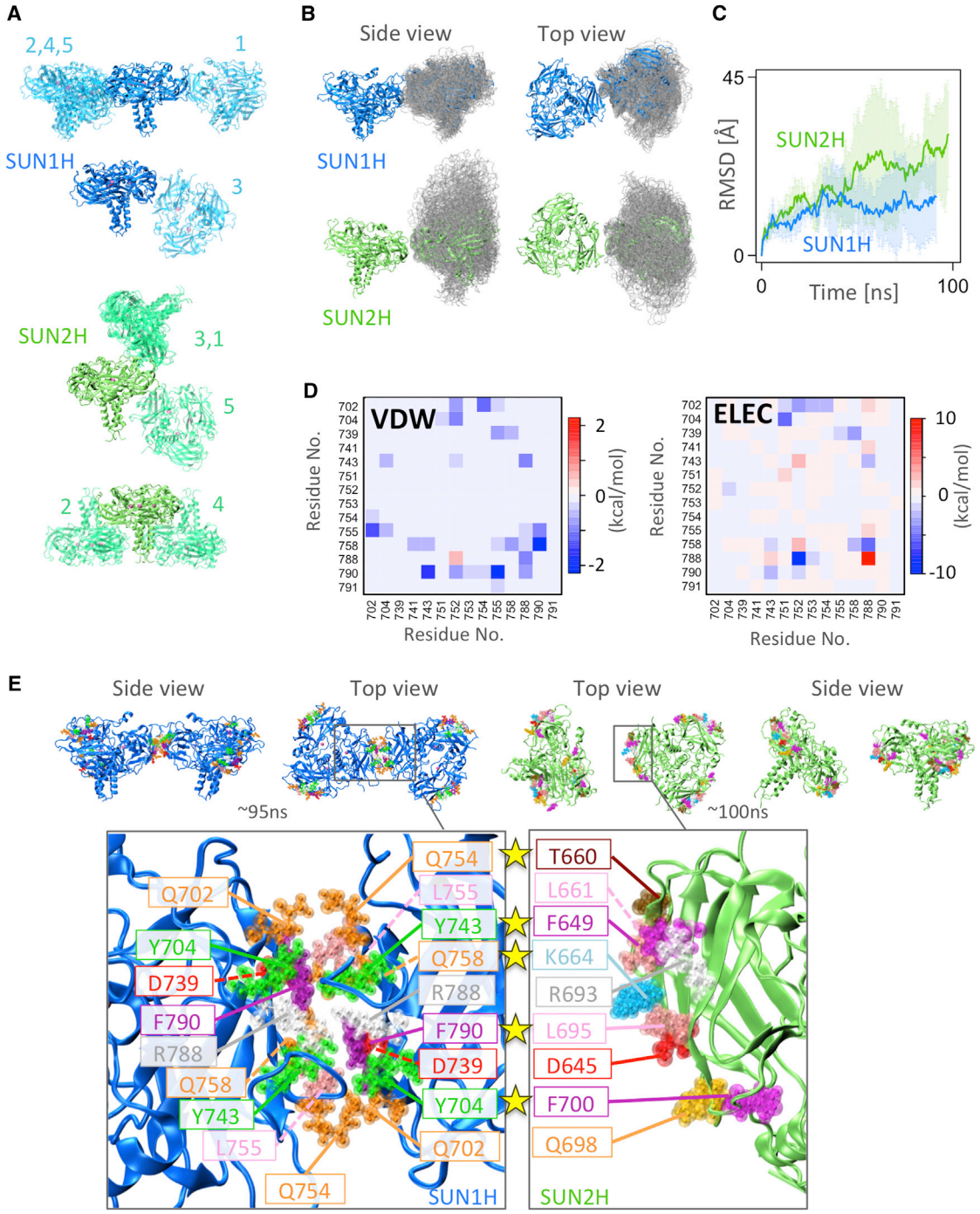

FIGURE 4 Lateral interaction of SUN1 trimers through their SUN domains. (*A*) Shown are the top five molecular docking results (ZDOCK server) between two SUN1 or two SUN2 trimers. Similar results are clustered and shown together, and each number (1–5) corresponds to the rank of the docking results. (*B*) Shown is a visualization of molecular dynamics trajectories of SUN1 and SUN2 homotrimers with respect to the neighboring trimer in SUN1H and human SUN2. (*C*) Shown is the average Cα-atom RMSD of a human SUN homotrimer with respect to the neighboring trimer in SUN1H and human SUN2. (*D*) Pairwise VDW (*left*) and ELEC (*right*) interaction energies between residue pairs within a 4Å distance on two SUN1H homotrimers are shown. (*E*) Shown is the final frame of the MD trajectory of lateral interaction simulations of SUN1 (95 ns) or SUN2 (100 ns); also shown is a close view of interacting residues at the interface of two SUN1H homotrimers (*blue*) and the corresponding surface on SUN2 homotrimers (*green*). Yellow stars indicate the residues that are different between SUN1 and SUN2 at this interface. ELEC, electrostatic. To see this figure in color, go online.

of our MD simulations (Fig. S3 *A*) and calculated their pairwise interaction energies (Fig. 4 *D*). Residues with significant VDW or ELEC interactions among all simulation runs were identified and are indicated in Fig. 4 *E*. No such interfaces were identified in our SUN2 homotrimer-homotrimer simulations (Fig. S3 *B*); however, the same interface

identified on SUN1 was mapped onto the structure of SUN2, and residues at this interface that were different between SUN1 and SUN2 were highlighted (Fig. 4 *E*).

KASH lid inhibition in SUN1 compared with SUN2

Having predicted that the α3-SUN domain of SUN1 is similar to SUN2, we next asked if the KASH lid of a SUN1 monomer might also be autoinhibited by an interaction with the three-helix bundle formed by α1, α2, and α3, as it is in SUN2 (46). To do this, we homology modeled SUN1M monomers using the recently solved monomeric structure of SUN2M (PDB: 5ed8) as a template (Fig. 5 *A*). Our SUN1M monomer model and the SUN2M monomeric structure were subjected to 90–100 ns MD simulations. Both monomeric SUN1M and SUN2M showed high RMSD values in their α1–3 helix bundle (Fig. 5 *B*). However, significantly higher RMSD values were observed in the α2 helix of SUN1M as compared to SUN2M (Fig. 5 *C*).

We then performed a one-to-one map of all nonconserved and semiconserved substitutions between SUN1 and SUN2 sequences on α1 and α2 domains of the refined modeled structures of monomeric SUN1M and SUN2M (Fig. 5 *D*). The α1 regions of SUN1M and SUN2M contained a high level of similar residues (35% identity and 53% similarity). And despite a low overall sequence similarity between the α2 regions of SUN1M and SUN2M (0% identity and 33.3% similarity), the main hydrophobic residues on α1 and α2 of SUN2M important for three-helix bundle formation, as identified by Nie et al. (46), are either identical or conservatively substituted in SUN1M (with the exception of H513 in the linker region of SUN2M, which is substituted with M694 in SUN1M) (Fig. 5 *D*).

Next, we compared the monomeric SUN1M and SUN2M models by calculating the total nonbonded interaction energies between their KASH lids and α1–3 helix bundles (Figs. 6, *A* and *B* and S3). The nonbonded interaction energies calculated for the interaction between the KASH lid and α1 helix were not significantly different between SUN1M and SUN2M. In addition, the α2 helix did not appear to interact with the KASH lid in either SUN protein.

To begin to define the mechanism responsible for the autoinhibition of the SUN1M SUN domain, we sought to identify the residues that contribute to the ELEC interaction energies between the KASH lid and the α1–3 helix bundle. We first asked if the previously described three-residue network that exists between the KASH lid (Y597), the α1 (E503) helix, and the α3 (R552) helix in SUN2M is also critical for the autoinhibition of SUN1M (46). Nie et al. (46) showed that a E503A mutation resulted in the activation of SUN2M for KASH binding in vitro. Additionally, this mutant could marginally increase the localization of KASH2 to the NE in vivo, demonstrating the importance of the three-residue network in SUN2M activation (46). To compare with SUN2M, we mapped the corresponding three residues onto the structure of SUN1M (Fig. 6 *C*). Indeed, E684 (E503 in SUN2M) is conserved in SUN1M and positioned perfectly to interact with Y779 (Y597 in SUN2M) through ELEC interactions and hydrogen bonding (Figs. 6, *C* and *D* and S3). However, the third residue of this network (R552 in SUN2M) is nonconservatively substituted with L734 at the same position on SUN1M, which results in the absence of the salt bridge observed between the α1 and α3 helices of SUN2M.

To further investigate the autoinhibitory role of these three residues in SUN1M and SUN2M, we calculated their pairwise interaction energies (Figs. 6 *D* and S3). Although the SUN1M α3 helix remained in contact with the KASH lid through ELEC and hydrogen binding of E684 and Y779, the interaction between the α3 and α1 helices was lost because of the absence of the salt bridge between E684 and L734 (Figs. 6 *D* and S3). The lack of this salt bridge also resulted in small shifts in the positions of the α1 and α2 helices relative to the KASH lid in SUN1M as compared to SUN2M (Figs. 6, *E* and S3). In addition, we measured smaller angles between the α1 and α2 helices as well as between the α1 helix and the KASH lid in SUN1M as opposed to SUN2M (Figs. 6, *F* and S3). These results suggest that the autoinhibition of the KASH lid may be weaker in SUN1M as compared with SUN2M.

DISCUSSION

Here, we provide, to our knowledge, novel insights into the structure and molecular dynamics of the core LINC complex proteins SUN1 and SUN2. We provide evidence to support that the α3 helix and SUN domain of SUN1 also favor a trimeric state, which is consistent with the homotrimer being the fundamental functional state for SUN domain proteins (45). In addition, we identify a previously uncharacterized and highly conserved salt bridge that forms between the SUN domain of one protomer and the α3 helix of an adjacent protomer in both SUN1 and SUN2. We also show that like SUN2, the KASH lid of monomeric SUN1 may be kept in an autoinhibited state via interactions with the preceding α1–3 helix bundle. However, the mechanism of autoinhibition appears to differ between SUN1 and SUN2. Finally, we describe a potential mechanism to explain the differential SUN protein homo-oligomerization observed in cells.

SUN1 oligomerization

The high level of homology between the protomer interfaces of SUN1 and SUN2 (specifically in the SUN and α3 domains) and the similarities between SUN1 and SUN2 potential energies in our models over multiple MD simulation runs provide evidence that like SUN2, the α3-SUN domain of SUN1 also favors a trimeric state (Figs. 2 and 3). In addition to interactions between adjacent SUN domains and α3 helices, we identified three interprotomer salt bridges,

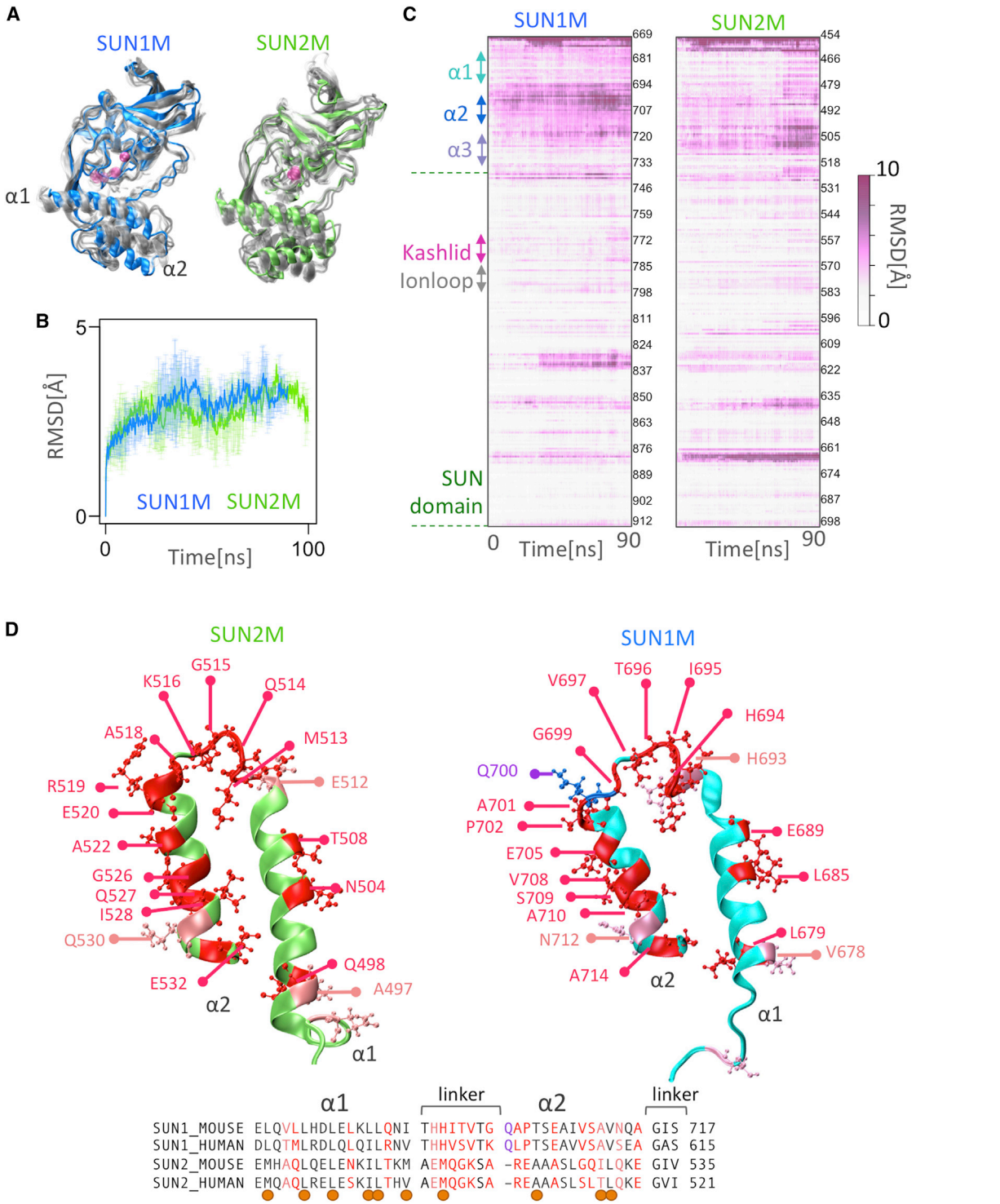

FIGURE 5 Structural models of monomeric (inactive) SUN1M and SUN2M. (*A*) Shown is a molecular dynamics trajectory visualization for SUN1M (*blue*) and SUN2M (*green*). Traces of the molecular dynamics trajectories of SUN1M and SUN2M trimers over the simulation time are shown in gray. (*B*) Shown is the average Cα-atom RMSD of SUN1M compared with SUN2M. All averages are obtained from three independent runs, and error bars correspond to standard deviations. (*C*) Shown are heatmaps of the average per-residue Cα-atom RMSD over time of SUN1M and SUN2M relative to the initial minimized modeled structures. All averages are obtained from three independent runs. (*D*) Shown is a one-to-one map of nonconserved residue substitutions between SUN1M and SUN2M on their α1 and α2 regions. Nonconserved residue substitutions on α1 and α2 of SUN1M compared with SUN2M are colored in red, semiconserved residues are colored in pink, and additional residues are colored in purple. Orange circles represent residues involved in three-helix bundle formation in monomeric mouse SUN2 as identified by Nie et al. (46). To see this figure in color, go online.

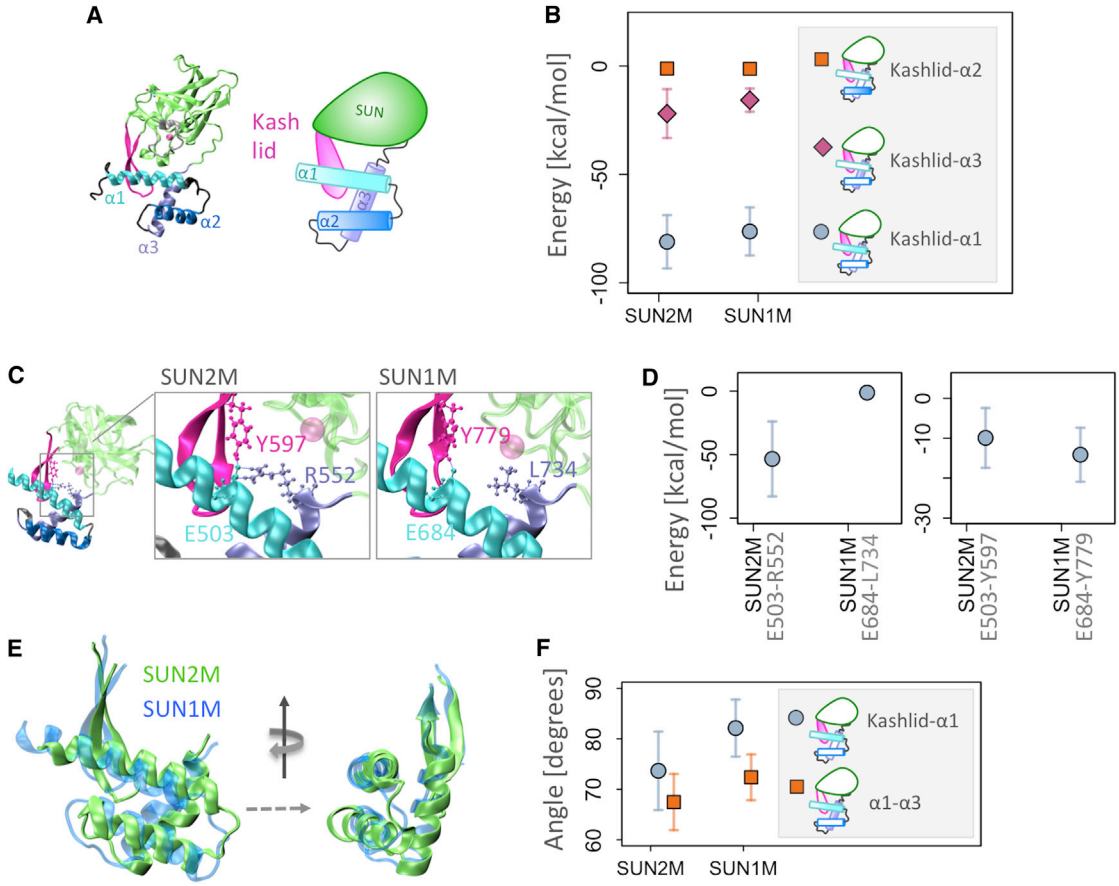

FIGURE 6 Inhibition of the KASH lid by the α-1–3 helix bundle in SUN1M and SUN2M. (*A*) Shown is an illustration of the inactive mouse SUN2 (SUN2M) domain architecture in which the KASH lid (*magenta*) is bound between a helix bundle formed by α1 (*cyan*), α2 (*blue*), and α3 (*purple*). (*B*) Shown are the total nonbonded interaction energies between the KASH lid and α1–3 helices. (*C*) Shown is a combined space-filling calotte (CPK) and ribbon representation of the three main residues responsible for bridging α1, α3 and the KASH lid identified in SUN2M (46) and their corresponding residues on SUN1M. (*D*) Shown are the interaction energies between the residues indicated in (*C*). (*E*) Shown is a superposition of α1–3 and the KASH lid of SUN1M and SUN2M. (*F*) Shown are the calculated angles between the indicated regions in (*E*). Here, nonbonded interaction energies and angles are averaged over MD simulation time and three independent runs, and error bars correspond to one standard deviation. To see this figure in color, go online.

one between the SUN domain of each protomer and the α3 helix of its neighboring protomer, in the modeled trimers of mouse and human SUN1 and SUN2 (Fig. 3, *C–E*). Judging by its conservation and it being the only interaction between SUN domains and neighboring α3 helices, we postulate that this salt bridge is important in maintaining the trimer stability. However, it is interesting to see whether disrupting this salt bridge could destabilize the trimers and affect KASH binding in vivo. In fact, there are multiple reports of salt bridges contributing to the stability of the active states of proteins that are capable of adopting various conformations (53–57). We must note that our methods only look at nonbonded potential energy similarities between SUN1 and SUN2 protomer interfaces and provide no information about the entropic costs or the conformational changes required for SUN1 or SUN2 to achieve a trimeric state. In fact, Sosa et al. (42) showed that the SUN domain of SUN2 is insufficient to form a stable trimer, and the preceding CC domains of SUN2 enforce this trimerization. However, they also showed that the SUN domain of SUN2 is only functional in a trimeric state (42,45) Therefore, a similar scenario is imaginable for SUN1 in which the SUN domain is functional in a trimeric form, but the CC regions are essential for trimerization, and further experiments are required to test this hypothesis.

If the SUN domains of SUN1 and SUN2 form trimers, how could one explain the observed assembly of SUN1 into even higher orders in the NE of living cells (34,58)? Our docking results and MD simulations suggest that SUN1 trimers could form higher-order clusters by a lateral association of their SUN domains (Figs. 4 and 7). In this model, each SUN1 protomer contains a docking site for a neighboring SUN1 trimer, giving rise to three sites on each trimer (Figs. 4 *E* and 7). Additionally, previous studies have shown that the CC-containing regions of the SUN1 luminal domain contain cysteine residues—C526 in SUN1H and C635 in SUN1M—that are capable of forming interchain disulfide bonds (34). In combination with our

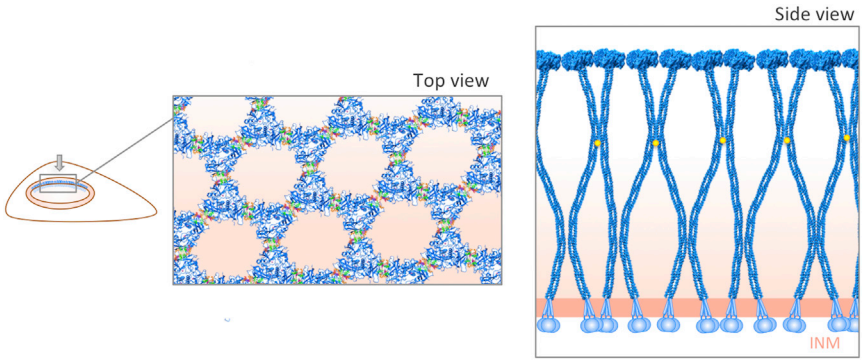

FIGURE 7 Hypothetical model of higher-order SUN protein oligomer assembly. Arrays of SUN1 proteins are formed or reinforced at the nuclear envelope by interactions between their SUN domains (*top view*). Residues on the surface of SUN1 that reinforce this interaction are colored and match the colors shown in Fig. 4 *E*. Additionally, the CC domain of SUN1 can associate through intertrimer disulfide bonds (*side view*). Yellow circles represent disulfide bonds between cysteine residues in the coiled-coil region of SUN1 (34). To see this figure in color, go online.

proposed SUN-domain docking sites, which would allow the SUN proteins to interact laterally through their SUN domains, such disulfides between trimers could lead to clusters of four SUN1 trimers also bound covalently through their CC regions to create large, immobile assemblies in the NE (Fig. 7). To understand the functional implications of SUN clustering in the NE, we draw a comparison between integrins, which are the transducers of mechanical signals at the cell membrane, and SUN domain proteins, which transmit signals across the INM. Integrin heterodimers are able to associate laterally in a process known as integrin clustering to form focal adhesions, which mediate bidirectional signaling between the extracellular matrix and cytoplasm (59). Not only is integrin clustering required for the formation of focal adhesions but it is also a determining factor in the strength of cell adhesions and the ability to sustain higher forces (59–61). Likewise, clustering of SUN proteins would enable them to sustain higher forces at the NE during various force-dependent processes such as chromosome movement and nuclear positioning (19,62).

Autoinhibition of the KASH lid in SUN1

We also asked whether SUN1, like SUN2, could adopt an inactive fold in which the SUN domain is bound to its preceding α-helical domains. Our results provide various indications of how molecular mechanisms of SUN1 activation and oligomerization may differ from that of SUN2. First, we identified a string of charged residues on the surface of SUN2 α3 that were all substituted with hydrophobic residues on SUN1 α3 (L632, A624, and A620 in SUN1H and L734, I726, and A722 in SUN1M) (Fig. 2 *B*). Despite indications of a trimeric α3-SUN domain of SUN1 in our models, we cannot eliminate the possibility of an alternative arrangement of the α3 regions of SUN1 that would bury these residues. It is possible that these residues on SUN1 α3 are involved in the inhibition of the KASH lid in the protein's inactive state.

Secondly, we show that an important three-residue cross-bridge between α1, α3, and the KASH lid is missing one component in SUN1 (R552 in SUN2M is substituted with L734 in SUN1M, as shown in Fig. 6 *C*). Thirdly, we showed that the hydrophobic residues on α1, α2, and α3 that are responsible for three-helix bundle formation on SUN2 are highly conserved in SUN1. Therefore, our models predict that α1, α2, and α3 domains are involved in KASH lid inhibition in SUN1, but this inhibition may be weaker than that of SUN2 because of the lack of a conserved substitution of R552 of SUN2M in SUN1M (Figs. 6 and S3). The differential inhibitory mechanisms of the SUN1 SUN domain as compared with SUN2 suggest that SUN1 and SUN2 may also be activated via different mechanisms, which could have various implications in the context of their distinct cellular processes. For example, a recent study suggested that SUN1 may inhibit RhoA activation by limiting the activity of SUN2, suggesting that SUN1 and SUN2 may compete for KASH binding (63). The absence of a salt bridge between the KASH lid and SUN1 α3 might suggest that the KASH lid is more readily available for KASH binding in SUN1 and hence would win in competition with SUN2.

Finally, we cannot overlook the possibility of different mechanisms of LINC formation and function across organisms. For example, contrary to all published data on human and mouse LINC complexes, Daryabeigi et al. (64) recently showed that in *Caenorhabditis elegans*, the oligomerization of SUN1 is not required for the formation of a functional LINC complex. It would be interesting to see how altered oligomerization states could relate to the diverse functions of these highly conserved SUN domain proteins across organisms (65).

SUPPORTING MATERIAL

Four figures and two tables are available at http://www.biophysj.org/biophysj/supplemental/S0006-3495(18)30141-3.

AUTHOR CONTRIBUTIONS

Z.J. and M.R.K.M. designed the experiments. Z.J., D.F., U.T.V., and E.A. performed the experiments. All authors analyzed the data and wrote the manuscript. M.R.K.M. contributed materials and analysis tools.

ACKNOWLEDGMENTS

We gratefully acknowledge discussions with and suggestions by Hengameh Shams and other members of the Molecular Cell Biomechanics Laboratory.

This work was supported by the National Science Foundation through grant CBET-0955291. In addition, this research used resources of the National Energy Research Scientific Computing Center, a Department of Energy Office of Science user facility supported by the Office of Science of the U.S. Department of Energy under contract No. DE-AC02-05CH11231.

REFERENCES

1. Starr, D. A., and M. Han. 2002. Role of ANC-1 in tethering nuclei to the actin cytoskeleton. *Science.* 298:406–409.
2. Padmakumar, V. C., T. Libotte, …, I. Karakesisoglou. 2005. The inner nuclear membrane protein Sun1 mediates the anchorage of Nesprin-2 to the nuclear envelope. *J. Cell Sci.* 118:3419–3430.
3. Crisp, M., Q. Liu, …, D. Hodzic. 2006. Coupling of the nucleus and cytoplasm: role of the LINC complex. *J. Cell Biol.* 172:41–53.
4. Haque, F., D. J. Lloyd, …, S. Shackleton. 2006. SUN1 interacts with nuclear lamin A and cytoplasmic nesprins to provide a physical connection between the nuclear lamina and the cytoskeleton. *Mol. Cell. Biol.* 26:3738–3751.
5. Lombardi, M. L., D. E. Jaalouk, …, J. Lammerding. 2011. The interaction between nesprins and sun proteins at the nuclear envelope is critical for force transmission between the nucleus and cytoskeleton. *J. Biol. Chem.* 286:26743–26753.
6. Gundersen, G. G., and H. J. Worman. 2013. Nuclear positioning. *Cell.* 152:1376–1389.
7. Khatau, S. B., C. M. Hale, …, D. Wirtz. 2009. A perinuclear actin cap regulates nuclear shape. *Proc. Natl. Acad. Sci. USA.* 106:19017–19022.
8. Stroud, M. J., I. Banerjee, …, J. Chen. 2014. LINC complex proteins in cardiac structure, function, and disease. *Circ. Res.* 114:538–548.
9. Yang, L., M. Munck, …, S. Neumann. 2013. Mutations in LMNA modulate the lamin A–Nesprin-2 interaction and cause LINC complex alterations. *PLoS One.* 8:e71850.
10. Méjat, A., and T. Misteli. 2010. LINC complexes in health and disease. *Nucleus.* 1:40–52.
11. Folker, E. S., and M. K. Baylies. 2013. Nuclear positioning in muscle development and disease. *Front. Physiol.* 4:363.
12. Meinke, P., T. D. Nguyen, and M. S. Wehnert. 2011. The LINC complex and human disease. *Biochem. Soc. Trans.* 39:1693–1697.
13. Meinke, P., E. Mattioli, …, S. Shackleton. 2014. Muscular dystrophy-associated SUN1 and SUN2 variants disrupt nuclear-cytoskeletal connections and myonuclear organization. *PLoS Genet.* 10:e1004605.
14. Haque, F., D. Mazzeo, …, S. Shackleton. 2010. Mammalian SUN protein interaction networks at the inner nuclear membrane and their role in laminopathy disease processes. *J. Biol. Chem.* 285:3487–3498.
15. Isermann, P., and J. Lammerding. 2013. Nuclear mechanics and mechanotransduction in health and disease. *Curr. Biol.* 23:R1113–R1121.
16. Puckelwartz, M. J., E. J. Kessler, …, E. M. McNally. 2010. Nesprin-1 mutations in human and murine cardiomyopathy. *J. Mol. Cell. Cardiol.* 48:600–608.
17. Matsumoto, A., M. Hieda, …, N. Matsuura. 2015. Global loss of a nuclear lamina component, lamin A/C, and LINC complex components SUN1, SUN2, and nesprin-2 in breast cancer. *Cancer Med.* 4:1547–1557.
18. Horn, H. F., Z. Brownstein, …, K. B. Avraham. 2013. The LINC complex is essential for hearing. *J Clin Invest.* 123:740–750.
19. Luxton, G. W., and D. A. Starr. 2014. KASHing up with the nucleus: novel functional roles of KASH proteins at the cytoplasmic surface of the nucleus. *Curr. Opin. Cell Biol.* 28:69–75.
20. Kim, D. I., K. C. Birendra, and K. J. Roux. 2015. Making the LINC: SUN and KASH protein interactions. *Biol Chem.* 396:295–310.
21. Malone, C. J., W. D. Fixsen, …, M. Han. 1999. UNC-84 localizes to the nuclear envelope and is required for nuclear migration and anchoring during C. elegans development. *Development.* 3181:3171–3181.
22. Chang, W., H. J. Worman, and G. G. Gundersen. 2015. Accessorizing and anchoring the LINC complex for multifunctionality. *J. Cell Biol.* 208:11–22.
23. Nishioka, Y., H. Imaizumi, …, M. Hieda. 2016. SUN1 splice variants, SUN1_888, SUN1_785, and predominant SUN1_916, variably function in directional cell migration. *Nucleus.* 7:572–584.
24. Rajgor, D., and C. M. Shanahan. 2013. Nesprins: from the nuclear envelope and beyond. *Expert Rev. Mol. Med.* 15:e5.
25. Meinke, P., and E. C. Schirmer. 2015. LINC'ing form and function at the nuclear envelope. *FEBS Lett.* 589:2514–2521.
26. Duong, N. T., G. E. Morris, …, I. Holt. 2014. Nesprins: tissue-specific expression of epsilon and other short isoforms. *PLoS One.* 9:e94380.
27. Roux, K. J., M. L. Crisp, …, B. Burke. 2009. Nesprin 4 is an outer nuclear membrane protein that can induce kinesin-mediated cell polarization. *Proc. Natl. Acad. Sci. USA.* 106:2194–2199.
28. Zhang, X., K. Lei, …, M. Han. 2009. SUN1/2 and Syne/Nesprin-1/2 complexes connect centrosome to the nucleus during neurogenesis and neuronal migration in mice. *Neuron.* 64:173–187.
29. Wilhelmsen, K., S. H. Litjens, …, A. Sonnenberg. 2005. Nesprin-3, a novel outer nuclear membrane protein, associates with the cytoskeletal linker protein plectin. *J. Cell Biol.* 171:799–810.
30. Yu, J., K. Lei, …, M. Han. 2011. KASH protein Syne-2/Nesprin-2 and SUN proteins SUN1/2 mediate nuclear migration during mammalian retinal development. *Hum. Mol. Genet.* 20:1061–1073.
31. Morimoto, A., H. Shibuya, …, Y. Watanabe. 2012. A conserved KASH domain protein associates with telomeres, SUN1, and dynactin during mammalian meiosis. *J. Cell Biol.* 198:165–172.
32. Lei, K., X. Zhang, …, M. Han. 2009. SUN1 and SUN2 play critical but partially redundant roles in anchoring nuclei in skeletal muscle cells in mice. *Proc. Natl. Acad. Sci. USA.* 106:10207–10212.
33. Lei, K., X. Zhu, …, M. Han. 2012. Inner nuclear envelope proteins SUN1 and SUN2 play a prominent role in the DNA damage response. *Curr. Biol.* 22:1609–1615.
34. Lu, W., J. Gotzmann, …, I. Karakesisoglou. 2008. Sun1 forms immobile macromolecular assemblies at the nuclear envelope. *Biochim. Biophys. Acta.* 1783:2415–2426.
35. Li, P., and A. A. Noegel. 2015. Inner nuclear envelope protein SUN1 plays a prominent role in mammalian mRNA export. *Nucleic Acids Res.* 43:9874–9888.
36. Liu, Q., N. Pante, …, K. J. Roux. 2007. Functional association of Sun1 with nuclear pore complexes. *J. Cell Biol.* 178:785–798.
37. Horn, H. F., D. I. Kim, …, K. J. Roux. 2013. A mammalian KASH domain protein coupling meiotic chromosomes to the cytoskeleton. *J. Cell Biol.* 202:1023–1039.
38. Talamas, J. A., and M. W. Hetzer. 2011. POM121 and Sun1 play a role in early steps of interphase NPC assembly. *J. Cell Biol.* 194:27–37.
39. Ding, X., R. Xu, …, M. Han. 2007. SUN1 is required for telomere attachment to nuclear envelope and gametogenesis in mice. *Dev Cell.* 12:863–872.
40. Luxton, G. W. G., E. R. Gomes, …, G. G. Gundersen. 2010. Linear arrays of nuclear envelope proteins harness retrograde actin flow for nuclear movement. *Science.* 329:956–959.
41. Wang, Q., X. Du, …, M. I. Greene. 2006. Characterization of the structures involved in localization of the SUN proteins to the nuclear envelope and the centrosome. *DNA Cell Biol.* 25:554–562.
42. Sosa, B. A., A. Rothballer, …, T. U. Schwartz. 2012. LINC complexes form by binding of three KASH peptides to domain interfaces of trimeric SUN proteins. *Cell.* 149:1035–1047.
43. Zhou, Z., X. Du, …, Q. Wang. 2012. Structure of Sad1-UNC84 homology (SUN) domain defines features of molecular bridge in nuclear envelope. *J. Biol. Chem.* 287:5317–5326.

44. Wang, W., Z. Shi, …, Z. Zhou. 2012. Structural insights into SUN-KASH complexes across the nuclear envelope. *Cell Res.* 22:1440–1452.

45. Sosa, B. A., U. Kutay, and T. U. Schwartz. 2013. Structural insights into LINC complexes. *Curr. Opin. Struct. Biol.* 23:285–291.

46. Nie, S., H. Ke, …, W. Feng. 2016. Coiled-coil domains of SUN proteins as intrinsic dynamic regulators. *Structure.* 24:80–91.

47. The UniProt Consortium. 2017. UniProt: the universal protein knowledgebase. *Nucleic Acids Res.* 45:D158–D169.

48. Biasini, M., S. Bienert, …, T. Schwede. 2014. SWISS-MODEL: modelling protein tertiary and quaternary structure using evolutionary information. *Nucleic Acids Res.* 42:W252–W258.

49. Humphrey, W., A. Dalke, and K. Schulten. 1996. VMD: visual molecular dynamics. *J. Mol. Graph.* 14:33–38, 27–28.

50. Pierce, B. G., K. Wiehe, …, Z. Weng. 2014. ZDOCK server: interactive docking prediction of protein – protein complexes and symmetric multimers. *Bioinformatics.* 30:1771–1773.

51. Phillips, J. C., R. Braun, …, K. Schulten. 2005. Scalable molecular dynamics with NAMD. *J. Comput. Chem.* 26:1781–1802.

52. Zhou, X., K. Graumann, …, I. Meier. 2012. Novel plant SUN-KASH bridges are involved in RanGAP anchoring and nuclear shape determination. *J. Cell Biol.* 196:203–211.

53. Wang, W., T. Rasmussen, …, J. H. Naismith. 2012. Salt bridges regulate both dimer formation and monomeric flexibility in HdeB and may have a role in periplasmic chaperone function. *J. Mol. Biol.* 415:538–546.

54. Wei, Q., S. Yang, …, Z. Jia. 2016. A new autoinhibited kinase conformation reveals a salt-bridge switch in kinase activation. *Sci. Rep.* 6:28437.

55. Dey, M., C. Cao, …, T. E. Dever. 2007. Conserved intermolecular salt bridge required for activation of protein kinases PKR, GCN2, and PERK. *J. Biol. Chem.* 282:6653–6660.

56. Mehrbod, M., S. Trisno, and M. R. Mofrad. 2013. On the activation of integrin αIIbβ3: outside-in and inside-out pathways. *Biophys. J.* 105:1304–1315.

57. P Barros, E., R. D. Malmstrom, …, R. E. Amaro. 2017. Electrostatic interactions as mediators in the allosteric activation of protein kinase A RIα. *Biochemistry.* 56:1536–1545.

58. Hennen, J., K. H. Hur, …, J. D. Mueller. 2017. Quantitative brightness analysis of protein oligomerization in the nuclear envelope. *Biophys. J.* 113:138–147.

59. Jamali, Y., T. Jamali, and M. R. K. Mofrad. 2012. An agent based model of integrin clustering: exploring the role of ligand clustering, integrin homo-oligomerization, integrin-ligand affinity, membrane crowdedness and ligand mobility. *Journal of Computational Physics.* 244:264–278.

60. Mehrbod, M., and M. R. Mofrad. 2013. Localized lipid packing of transmembrane domains impedes integrin clustering. *PLOS Comput. Biol.* 9:e1002948.

61. Jahed, Z., H. Shams, …, M. R. Mofrad. 2014. Mechanotransduction pathways linking the extracellular matrix to the nucleus. *Int. Rev. Cell Mol. Biol.* 310:171–220.

62. Jahed, Z., H. Shams, and M. R. Mofrad. 2015. A disulfide bond is required for the transmission of forces through SUN-KASH complexes. *Biophys. J.* 109:501–509.

63. Thakar, K., C. K. May, …, C. W. Carroll. 2017. Opposing roles for distinct LINC complexes in regulation of the small GTPase RhoA. *Mol Biol Cell.* 28:182–191.

64. Daryabeigi, A., A. Woglar, …, V. Jantsch. 2016. Nuclear envelope retention of LINC complexes is promoted by SUN-1 oligomerization in the caenorhabditis elegans germ line. *Genetics.* 203:733–748.

65. Jahed, Z., and Mofrad, M.R.K. Mechanical LINCs of the nuclear envelope: where SUN meets KASH. *Extreme Mechanics Letters.* 20:99–103.